J. Fluid Mech. (1985), *vol.* 157, *pp.* 471–492
Printed in Great Britain

Asymmetric flow above a rotating disk

By C.-Y. LAI, K. R. RAJAGOPAL AND A. Z. SZERI
Department of Mechanical Engineering, University of Pittsburgh, PA 15261

(Received 20 July 1984 and in revised form 13 February 1985)

In this paper we generalize the von Kármán solution for flow above a single rotating disk, to include non-axisymmetric solutions. These solutions contain an arbitrary parameter; for zero value of the parameter the asymmetric flow degenerates into the classical von Kármán solution. Thus the classical solution is never isolated when considered within the scope of the full Navier–Stokes equations; there are asymmetric solutions in every neighbourhood of the von Kármán solution. Calculations are reported here for $s = 0$, 0.02 and 0.06, where s represents the ratio of angular velocity of the fluid at infinity to the angular velocity of the disk. A subset of the solutions obtained here corresponds to flow induced by the rotation of a disk when the latter is placed in a fluid that is moving with a constant uniform velocity.

1. Introduction

The problem of disk flows has occupied a central position in fluid mechanics ever since the pioneering work of von Kármán (1921). The reason for this, one suspects, is that the geometry of the flow is one of the simplest possible. Correspondingly, one might presume the right to have an uncomplicated flow, even though the flow is described by equations in which the nonlinear terms have been retained. This expectation almost seemed to be fulfilled when von Kármán first showed that two simple propositions, viz that the flow is axisymmetric and that the axial velocity is independent of the radial coordinate, reduce the equations of motion to a set of ordinary differential equations.

The similarity transformation that results from the von Kármán postulates remains applicable even when the fluid at infinity is rotating about the axis of the disk. Solutions have been obtained for various values of s by Rogers & Lance (1960) and others. However, it appeared to be impossible to find solutions in the range $-0.160 > s > -1.4351$. It is now clear that at $s = -1.4351$ the solution of the equations becomes singular. At $s = -0.160$ the situation was more mysterious. Weidman & Redekopp (1975) suggested that a singularity exists in this neighbourhood. The speculation ended with the work of Zandbergen & Dijkstra (1977) and Dijkstra (1980), who showed that branching occurs at $s = -0.16054$. They discussed the two branches that coincide here, and conjectured that there are an infinite number of solutions to the problem in a small region near $s = 0$. Lentini & Keller (1980*a*, *b*) found that at least four families of solutions exist and indicated the possibility of the existence of an infinite sequence of solutions. The main difference between the solutions is an extra cell, which is built up as the solution proceeds from one branch into another. Near the disk and near infinity the solutions are almost indistinguishable, particularly when higher branches are compared. Flows with $s = 0$, having zero angular velocity at infinity, exist in each family.

Theoretical investigations have been carried out by Hastings (1970), McLeod (1971) and Lan (1971), among others. The asymptotic behaviour of the solution at infinity,

which is of fundamental importance in obtaining solutions, was first investigated by Rogers & Lance (1960) and later by McLeod (1969), who showed rigorously that the decay is exponential; it is monotonic for $s = 0$, while $s \neq 0$ leads to oscillatory behaviour as $z \to \infty$. Lentini & Keller (1980*a*, *b*) made use of McLeod's work and investigated the condition that ensures bounded solutions. The condition is simply that the solution of the associated linear problem vanish when projected into the union of certain subspaces, the only subspace where it could grow out of bounds. This analysis leads to asymptotic conditions which are evaluated at some finite position z_∞.

Recently Berker (1979) considered the flow between corotating disks and established a one-parameter family of solutions. The only axisymmetric solution in this family is the rigid-body motion, thus it is just this solution that would follow from the von Kármán assumption. Further developing Berker's ideas, Parter & Rajagopal (1984) proved the existence of a one-parameter family of solutions for flow between two disks. The only axisymmetric solutions are the von Kármán solutions. These solutions were calculated by Lai, Rajagopal & Szeri (1984).

In the light of the foregoing, one is advised to reexamine the classical problem of flow over a single rotating disk, within the context of establishing asymmetric solutions. For the form of the velocity field sought it is found that the set of governing equations contain, in addition to the nonlinear equations of axisymmetric flow, two coupled linear equations. The coefficients of the linear equations depend on the solution of the axisymmetric problem. The axisymmetric flow that is investigated here is the result of superposition, in each $z =$ constant plane, of the von Kármán swirling flow and a velocity of translation, the latter containing an arbitrary parameter C. For a given value of this parameter, the velocity of translation is different in each plane. The asymmetric solution is continuous in C; thus symmetric solutions of the von Kármán problem are never isolated when considered within the scope of the full Navier–Stokes equations.

In this paper we present asymmetric solutions over a single rotating disk at three values, $s = 0$, 0.02 and 0.06, of the velocity ratio. At the first of these s-values, i.e. for non-rotating flow at infinity, we have

$$\lim_{z \to \infty} \frac{|\boldsymbol{q}|}{|\boldsymbol{V}|} = \infty \quad (s = 0),$$

where $\boldsymbol{V}(x^1, x^3) = \{U, V, W\}$ represents the von Kármán solution and $\boldsymbol{q}(z) = \{q_r, q_\theta, 0\}$ is the rigid-body translation; the distance between the locus of stagnation points† and the axis of rotation grows out of bound as $z \to \infty$. For $s \neq 0$, however, $\boldsymbol{V}(z) \neq 0$ as $z \to \infty$, and returns into the axis of rotation as $z \to \infty$.

2. Analysis

The flow field is located above, and is limited by a single disk of infinite radius. The disk occupies the $x^3 = 0$ position in a cylindrical polar coordinate system $\{x^1, x^2, x^3\}$. We further define a non-dimensional coordinate system $\{r, \theta, z\}$ through

$$r = \left(\frac{\omega}{\nu}\right)^{\frac{1}{2}} x^1, \quad \theta = x^2, \quad z = \left(\frac{\omega}{\nu}\right)^{\frac{1}{2}} x^3. \tag{1}$$

† Stagnation point is defined here through $q_r + U = q_\theta + V = 0$.

The disk is rotating with angular velocity ω, the kinematic viscosity of the fluid is ν and the angular velocity of the fluid as $z \to \infty$ is $s\omega$.

Von Kármán (1921) searched for axisymmetric solutions to the flow induced by the rotation of the disk. The assumption that the axial velocity component is uniform over z = constant planes and that the flow is independent of the azimuthal coordinate yields the following velocity field for the von Kármán swirling-flow problem:

$$\left.\begin{aligned} U &= x^1 \omega F(x^3), \\ V &= x^1 \omega G(x^3), \\ W &= (\nu\omega)^{\frac{1}{2}} H(x^3) \end{aligned}\right\} \tag{2}$$

Here $V(x^1, x^3) = \{U, V, W\}$ is the velocity of the axisymmetric flow, which is further required to satisfy the constraint of incompressibility

$$\operatorname{div} V = 0. \tag{3}$$

Equation (3) leads to the condition

$$F(z) = -\frac{1}{2}\frac{\mathrm{d}H}{\mathrm{d}z}, \tag{4}$$

and this, together with (2), yields von Kármán's equations upon substitution into the Navier–Stokes equations:

$$\frac{\mathrm{d}^3 H}{\mathrm{d}z^3} - H\frac{\mathrm{d}^2 H}{\mathrm{d}z^2} + \frac{1}{2}\left(\frac{\mathrm{d}H}{\mathrm{d}z}\right)^2 - 2G^2 + 2s^2 = 0, \tag{5a}$$

$$\frac{\mathrm{d}^2 G}{\mathrm{d}z^2} - H\frac{\mathrm{d}G}{\mathrm{d}z} + G\frac{\mathrm{d}H}{\mathrm{d}z} = 0. \tag{5b}$$

The boundary conditions that accompany (5*a*, *b*) are as follows:

$$H = \frac{\mathrm{d}H}{\mathrm{d}z} = 0, \quad G = 1 \quad \text{at } z = 0, \tag{6a}$$

$$\frac{\mathrm{d}H}{\mathrm{d}z} \to 0, \quad G \to s \quad \text{at } z \to \infty. \tag{6b}$$

To make the problem determinate (Rogers & Lance 1960) it was also necessary to assume that

$$\frac{\mathrm{d}^2 H}{\mathrm{d}z^2}, \frac{\mathrm{d}^3 H}{\mathrm{d}z^3} \to 0 \quad \text{as } z \to \infty. \tag{7}$$

This condition is, in fact, responsible for the appearance of s, the ratio of rotational speeds, in (5*a*).

The von Kármán problem, represented by (5)–(7), has been solved by several investigators. We mention here only two recent solutions. Zandbergen & Dijkstra (1977) employed two methods. Their first method was a finite-difference discretization of the boundary-value problem equation (5), (6) and (7) on a uniform mesh, followed by Newton's method to solve the resulting set of nonlinear algebraic equations. Their second method was a shooting technique; in this the equations were integrated inward from some finite value of z, say z_∞, at which position the values for H, H', H'', G and G' were obtained from the second-order asymptotic approximations of Rogers & Lance (1960). The asymptotic approximation was calculated from a small perturbation of the solid-body rotation. Lentini & Keller (1980), on the other hand, treated (5)

as a two-point boundary value problem with boundary conditions (6*a*) prescribed at $z = 0$ and the following asymptotic conditions specified at some z_∞:

$$[H_\infty + a(H_\infty, s)]\frac{\mathrm{d}H}{\mathrm{d}z}\bigg|_{z_\infty} + \frac{\mathrm{d}^2H}{\mathrm{d}z^2}\bigg|_{z_\infty} - \frac{s}{a(H_\infty, s)}[G(z_\infty) - s] = 0, \tag{8a}$$

$$\frac{b^2(H_\infty, s)}{s}a(H_\infty, s)\frac{\mathrm{d}H}{\mathrm{d}z}\bigg|_{z_\infty} + [H_\infty + a(H_\infty, s)][G(z_\infty) - s] + \frac{\mathrm{d}G}{\mathrm{d}z}\bigg|_{z_\infty} = 0, \tag{8b}$$

where

$$a(H_\infty, s) = \frac{1}{\sqrt{2}}[(H_\infty^4 + 4s^2)^{\frac{1}{2}} + H_\infty^2]^{\frac{1}{2}}, \tag{9a}$$

$$b(H_\infty, s) = \frac{1}{\sqrt{2}}[(H_\infty^4 + 4s^2)^{\frac{1}{2}} - H_\infty^2]^{\frac{1}{2}}, \tag{9b}$$

and $H_\infty = H(z_\infty)$ is the (unknown) axial flow at z_∞.

Equations (8*a*, *b*) are the solvability conditions of the linear problem corresponding to (5), and ensure bounded solutions of the nonlinear problem on the semi-infinite interval $0 < z$ (Lentini & Keller 1978). The basic numerical scheme in the work of Lentini & Keller was to use finite differences on a non-uniform mesh, coupled with Newton's method.

In this paper we generalize the von Kármán solution to a set of asymmetric solutions, obtained when superposing a rigid-body motion of uniform velocity for each z = constant plane, on the spiral flow of the von Kármán solution. The resulting velocity field, when suitably non-dimensionalized, takes the form

$$\bar{u}(r, \theta, z) = F(z) + \frac{1}{r}[g(z)\cos\theta - f(z)\sin\theta], \tag{10a}$$

$$\bar{v}(r, \theta, z) = G(z) - \frac{1}{r}[g(z)\sin\theta + f(z)\cos\theta], \tag{10b}$$

$$\bar{w}(z) = H(z). \tag{10c}$$

Here

$$\{\bar{u}, \bar{v}, \bar{w}\} = \frac{1}{x^1\omega}\{u, v, rw\}, \tag{11}$$

and

$$\boldsymbol{v}(x^1, x^2, x^3) = \{u, v, w\}$$

is the velocity of the asymmetric flow, $\boldsymbol{v} = \boldsymbol{V}(x^1, x^3) + \boldsymbol{q}(x^2, x^3)$.

The velocity field (10*a*–*c*) satisfies the incompressibility constraint (3) if condition (4) is accepted, and when substituted into the full Navier–Stokes equation it yields the following set of ordinary differential equations:

$$\frac{\mathrm{d}^3H}{\mathrm{d}z^3} - H\frac{\mathrm{d}^2H}{\mathrm{d}z^2} + \frac{1}{2}\left(\frac{\mathrm{d}H}{\mathrm{d}z}\right)^2 - 2G^2 + 2s^2 = 0, \tag{12a}$$

$$\frac{\mathrm{d}^2G}{\mathrm{d}z^2} - H\frac{\mathrm{d}G}{\mathrm{d}z} + G\frac{\mathrm{d}H}{\mathrm{d}z} = 0, \tag{12b}$$

$$\frac{\mathrm{d}^3f}{\mathrm{d}z^3} - H\frac{\mathrm{d}^2f}{\mathrm{d}z^2} - \frac{1}{2}\frac{\mathrm{d}H}{\mathrm{d}z}\frac{\mathrm{d}f}{\mathrm{d}z} + \tfrac{1}{2}f\frac{\mathrm{d}^2H}{\mathrm{d}z^2} + \frac{\mathrm{d}}{\mathrm{d}z}(Gg) = 0, \tag{12c}$$

$$\frac{\mathrm{d}^3g}{\mathrm{d}z^3} - H\frac{\mathrm{d}^2g}{\mathrm{d}z^2} - \frac{1}{2}\frac{\mathrm{d}H}{\mathrm{d}z}\frac{\mathrm{d}g}{\mathrm{d}z} + \tfrac{1}{2}g\frac{\mathrm{d}^2H}{\mathrm{d}z^2} - \frac{\mathrm{d}}{\mathrm{d}z}(Gf) = 0. \tag{12d}$$

Equations of (12*a*, *b*) are identical with the von Kármán equations (5), while 12(*c*, *d*) give conditions on $f(z)$ and $g(z)$ such that $\boldsymbol{q}(\theta, z)$ be consistent with the Navier–Stokes

equations. Note that $\{(\nu\omega)^{\frac{1}{2}}g(z), -(\nu\omega)^{\frac{1}{2}}f(z)\}$ are the Cartesian components of the velocity field that is superposed on the von Kármán swirling flow.

To ensure that (12*a*, *b*) yield the von Kármán solution, we set

$$H = H' = 0, \quad G = 1 \quad \text{at } z = 0, \tag{13a}$$

$$H' \to 0, \quad G \to s \quad \text{as } z \to \infty. \tag{13b}$$

It now remains to specify boundary conditions for $\{f(z), g(z)\}$. At the disk we must require no slip, i.e.

$$f = g = 0 \quad \text{at } z = 0, \tag{13c}$$

but the remaining boundary conditions may be chosen in several different ways.

(i) If we choose

$$f \to C, \quad g \to 0 \quad \text{as } z \to \infty, \tag{14a}$$

we establish conditions for flow induced by a rotating disk as it is placed in a fluid that is moving with the uniform velocity $\{0, -(\nu\omega)^{\frac{1}{2}}C, 0\}$. To avoid a shear layer at infinity, we also set

$$f' \to 0, \quad g' \to 0 \quad \text{as } z \to \infty. \tag{14b}$$

(ii) One might also specify that

$$f \to 0, \quad g \to 0 \quad \text{as } z \to \infty, \tag{15a}$$

and that

$$f = C, \quad g = 0 \quad \text{at } z = l, \tag{15b}$$

where $z = l$ is some intermediate position. Although this family of solutions does not lend itself to immediate physical interpretation, it does represent hitherto unknown solutions to the Navier–Stokes equations, and as such deserves investigation.

Asymmetric flow between two parallel disks has been discussed in detail by Lai *et al.* (1984). The numerical study was based on the existence proofs of Parter & Rajagopal (1984). The extension of these proofs to flow above a single rotating disk is trivial (Parter & Rajagopal 1984), and we can thus ascertain that, whenever there is a solution to the von Kármán problem (5) and (7), there is also a solution to the system (12)–(14) for each C. Thus symmetric solutions of the problem of flow above a rotating disk are never isolated: there is an asymmetric solution arbitrarily close by.

Before the start of numerical work, we normalize the independent variable, $z \geqslant 0$, to $\bar{z} = z/z_\infty$, $0 \leqslant \bar{z} \leqslant 1$. Here z_∞ is some finite number; its precise value will be defined later. Correspondingly, (12*a–d*) are transformed to

$$H''' - z_\infty HH'' + \tfrac{1}{2}z_\infty H'^2 - 2z_\infty^3(G^2 - s^2) = 0, \tag{16a}$$

$$G'' - z_\infty(G'H - H'G) = 0, \tag{16b}$$

$$f''' - z_\infty Hf'' - \tfrac{1}{2}z_\infty H'f' + \tfrac{1}{2}z_\infty H''f + z_\infty^2(Gg)' = 0, \tag{16c}$$

$$g''' - z_\infty Hg'' - \tfrac{1}{2}z_\infty H'g' + \tfrac{1}{2}z_\infty H''g - z_\infty^2(Gf)' = 0. \tag{16d}$$

Here the prime signifies differentiation with respect to the normalized variable $\bar{z}$. The boundary conditions (13*a–c*) now take the form

$$H(0) = H'(0) = 0, \quad G(0) = 1, \tag{17a}$$

$$H'(1) = 0, \quad G(1) = s, \tag{17b}$$

$$f(0) = 0, \quad g(0) = 0, \tag{17c}$$

and either

$$f(1) = C, \quad g(1) = 0, \tag{18a}$$

$$f'(1) = 0, \quad g'(1) = 0, \tag{18b}$$

for the first family of solutions, or

$$f(1) = 0, \quad g(1) = 0, \tag{19a}$$

$$f(\bar{l}) = C, \quad g(\bar{l}) = 0. \tag{19b}$$

for the second family. In what follows we detail the analysis for the second family of solutions, (19*a*, *b*), only.

We have solved (16) in various ways and with varying accuracy. The method we describe in detail treats (16) as a boundary-value problem, but replaces conditions (19*a*) by the asymptotic conditions of Lentini & Keller (8); these asymptotic conditions are to be applied at a finite z_∞. The normalized form of these conditions is

$$\frac{1}{z_\infty}[H_\infty + a(H_\infty, s)]\, H'(1) + \frac{1}{z_\infty^2} H''(1) - \frac{s}{a(H_\infty, s)}[G_\infty - s] = 0, \tag{20a}$$

$$\frac{b^2(H_\infty, s)}{z_\infty s} a(H_\infty, s)\, H'(1) + [H_\infty + a(H_\infty, s)]\,(G_\infty - s) + \frac{1}{z_\infty} G'(1) = 0, \tag{20b}$$

where $H_\infty = H(1)$ and $G_\infty = G(1)$.

The asymptotic conditions on $H(z)$ and $G(z)$ of Lentini & Keller are nonlinear and enable computations to be made on shorter finite intervals than would otherwise be possible. This is particularly important when solving for higher branches of (16).

3. Numerical method

The development here parallels the corresponding development in Lai *et al.* (1984). We seek solutions of the system (12)–(16) in the weak form:

$$\{H(z), G(z), f(z), g(z)\} = \sum_{i=1}^{N} \{H_i, G_i, f_i, g_i\} B_i(z). \tag{21}$$

Here the $B_i(z)$, $1 \leqslant i \leqslant N$, are cubic B-splines defined over the partition

$$\pi: 0 = z_1 < z_2 < \ldots < z_{l+1} = 1, \tag{22}$$

with uniform smoothness $\gamma_i = \gamma = 3$, $2 \leqslant i \leqslant l$, on the interior breakpoints, and a knot sequence

$$\left.\begin{aligned} z_1 &= t_1 = t_2 = t_3 = t_4, \\ z_2 &= t_5, \\ &\vdots \\ z_l &= t_N \\ z_{l+1} &= t_{N+1} = t_{N+2} = t_{N+3} = t_{N+4}. \end{aligned}\right\} \tag{23}$$

The B-splines have the following relevant properties (de Boor 1978):

$$\left.\begin{aligned} B_1(z_1) = B_N(z_{l+1}) &= 1, \\ B_j(z_1) &= 0 \quad (j > 1), \\ B_j(z_{l+1}) &= 0 \quad (j < N); \end{aligned}\right\} \tag{24a}$$

$$\left.\begin{aligned} B_j(z) &= 0 \quad (z \notin [t_j, t_{j+4}]), \\ B_j(z) &\geqslant 0 \quad (z \in [0, 1]); \end{aligned}\right\} \tag{24b}$$

$$\left.\begin{aligned} B_1'(z_1) &= -B_2'(z_1) \neq 0, \\ B_j'(z_1) &= 0 \quad (j > 2), \\ B_N'(z_{l+1}) &= -B_{N-1}'(z_{l+1}) \neq 0, \\ B_j'(z_{l+1}) &= 0 \quad (j < N-1). \end{aligned}\right\} \tag{24c}$$

The approximation (21) can be made to satisfy the boundary conditions. It follows from (17) and (19) that

$$H_1 = H_2 = 0, \quad G_1 = 1, \tag{25a}$$

$$H_{N-1} = H_N, \quad G_N = 5, \tag{25b}$$

$$f_1 = f_2 = g_1 = g_N = 0, \tag{25c}$$

while condition (19*b*) leads to

$$\sum_{n=2}^{N-1} f_n B_n(\bar{l}) = C, \quad \sum_{n=2}^{N-1} g_n B_n(\bar{l}) = 0. \tag{26a, b}$$

The discretized forms of the Lentini & Keller asymptotic conditions (20*a*, *b*) are

$$\frac{1}{z_\infty}[H_N + a(H_N, s)](H_N - H_{N-1}) B_N'(\bar{z}_{l+1}) + \frac{1}{z_\infty^2}[H_{N-2} B_N''(\bar{z}_{l-1}) + H_{N-1} B_N''(\bar{z}_l) + H_N B_N''(\bar{z}_{l+1})] - \frac{s}{a(H_N, s)}(G_N - s) = 0, \tag{27a}$$

$$\frac{1}{z_\infty}\frac{b^2(H_N, s)}{s} a(H_N, s)(H_N - H_{N-1}) B_N'(\bar{z}_{l+1}) + [H_N + a(H_N, s)](G_N - s) + \frac{1}{z_\infty}(G_N - G_{N-1}) B_N'(\bar{z}_{l+1}) = 0, \tag{27b}$$

where

$$\left.\begin{aligned} a(H_N, s) &= \frac{1}{\sqrt{2}}[(H_N^4 + 4s^2)^{\frac{1}{2}} + H_N^2]^{\frac{1}{2}}, \\ b(H_N, s) &= \frac{1}{\sqrt{2}}[(H_N^4 + 4s^2)^{\frac{1}{2}} - H_N^2]^{\frac{1}{2}}. \end{aligned}\right\} \tag{28}$$

Substituting the expansions (20*a*, *b*) into (16*a–d*) and multiplying through by the test sets

$$\left.\begin{aligned} \tau^H &= \{B_m(\bar{z}) : 3 \leqslant m \leqslant N-1\}, \\ \tau^G &= \{B_n(\bar{z}) : 2 \leqslant n \leqslant N-1\}, \\ \tau^f &= \{B_k(\bar{z}) : 2 \leqslant k \leqslant N-2\}, \\ \tau^g &= \{B_l(\bar{z}) : 2 \leqslant l \leqslant N-2\}, \end{aligned}\right\} \tag{29}$$

and integrating with respect to $\bar{z}$, from $\bar{z} = 0$ to $\bar{z} = 1$, we obtain four sets of algebraic equations. Two of these sets are nonlinear and represent the von Kármán swirling flow. The other two are linear and contain f_i and g_i. The sets of equations can be written as follows:

$$\sum_{i=1}^{N}\left\{\frac{1}{z_\infty^3} H_i \bar{z}_{mi}^{(4)} - 2s^2 \bar{z}_{mi}^{(0)}\right\} + \sum_{i,j=1}^{N}\left\{\frac{1}{z_\infty^2} H_i H_j [\overline{Z}_{mij}^{(2)} - \tfrac{1}{2}\overline{Z}_{mij}^{(3)}] + 2G_i G_j \overline{Z}_{mij}^{(0)}\right\} = 0, \tag{30a}$$

$$\sum_{i=1}^{N} G_i \bar{z}_{ni}^{(2)} + z_\infty \sum_{i,j=1}^{N} G_i H_j (\overline{Z}_{nij}^{(1)} - \overline{Z}_{njl}^{(1)}) = 0, \tag{30b}$$

$$\sum_{j=1}^{N} f_j\left\{-\bar{z}_{kj}^{(4)} + z_\infty \sum_{i=1}^{N} H_i [\tfrac{1}{2}\overline{Z}_{kji}^{(2)} - \tfrac{1}{2}\overline{Z}_{kij}^{(3)} - \overline{Z}_{kij}^{(2)}]\right\} + z_\infty^2 \sum_{i,j=1}^{N} G_i g_j [\overline{Z}_{kji}^{(1)} + \overline{Z}_{kij}^{(1)}] = 0, \tag{30c}$$

$$-z_\infty^2 \sum_{i,j=1}^{N} G_i f_j [\bar{Z}_{lij}^{(1)} + \bar{Z}_{lji}^{(1)}] + \sum_{j=1}^{N} g_j \left\{ -\bar{z}_{lj}^{(4)} + z_\infty \sum_{i=1}^{N} H_i [\tfrac{1}{2}\bar{Z}_{lji}^{(2)} - \tfrac{1}{2}\bar{Z}_{lij}^{(3)} - \bar{Z}_{lij}^{(2)}] \right\} = 0, \quad (30d)$$

$$3 \leqslant m \leqslant N-1, \quad 2 \leqslant n \leqslant N-1, \quad 2 \leqslant k \leqslant N-2, \quad 2 \leqslant l \leqslant N-2.$$

Implicit in (30*a–d*) are the conditions (25*a*, *b*).

The Galerkin coefficients $\bar{z}_{jk}^{(0)}, \ldots, \bar{Z}_{ijk}^{(3)}$ are defined as follows:

$$\left.\begin{aligned} \bar{z}_{jk}^{(a)} &= \int_0^1 B_j^{(b)}(\bar{z})\, B_k^{(c)}(\bar{z})\, \mathrm{d}\bar{z}, \\ \bar{Z}_{ijk}^{(a)} &= \int_0^1 B_i^{(a)}(\bar{z})\, B_j^{(b)}(\bar{z})\, B_k^{(c)}(\bar{z})\, \mathrm{d}\bar{z}, \end{aligned}\right\} \quad (31)$$

$$a \leqslant b \leqslant c,$$

$$\alpha = a+b+c+1 \ (\text{if } b \neq 0)+2 \ (\text{if } a \neq 0).$$

The nonlinear algebraic system consisting of (25)–(27) and (30) was solved via a Newton-like method on the PDP-10 computer of the University of Pittsburgh. The splines and their derivatives were evaluated from recurrence relations, employing the subroutine package of de Boor (1978).

During the calculations the first solution is always obtained on a uniform breakpoint sequence. This solution is then improved by employing an adaptive mesh selection strategy of de Boor (Russell & Christiansen 1978). Let the solution $H(\bar{z})$ obtained on a uniform breakpoint distribution be represented by the cubic spline interpolation

$$P_n(\bar{z}) = \sum_{k=1}^{4} \frac{C_{k,n}}{n!} (\bar{z} - \tau_n)^{k-1}. \quad (32)$$

To evaluate the $C_{k,n}$ we use a subroutine (de Boor 1978) which requires the B-spline coefficients of the curve $H(\bar{z})$ as input, and on output supplies the interpolation coefficients. The calculation of the derivative of, say, $H(\bar{z})$ is based on the $C_{k,n}$, and we choose

$$h(\bar{z}) = \begin{cases} \dfrac{2|\Delta H_{\frac{3}{2}}|}{\bar{z}_3 - \bar{z}_1} & \text{on } [\bar{z}_1, \bar{z}_2], \\ \dfrac{|\Delta H_{i-\frac{1}{2}}|}{\bar{z}_{i+1} - \bar{z}_{i-1}} + \dfrac{|H_{i+\frac{1}{2}}|}{\bar{z}_{i+2} - \bar{z}_i} & \text{on } [\bar{z}_i, \bar{z}_{i+1}], \ 2 \leqslant i \leqslant l-1, \\ \dfrac{2|\Delta H_{l-\frac{1}{2}}|}{\bar{z}_{l+1} - \bar{z}_{l-1}} & \text{on } [\bar{z}_l, \bar{z}_{l+1}], \end{cases} \quad (33)$$

Here

$$\left.\begin{aligned} H_{i+\frac{1}{2}} &= H^{(k-1)}(\bar{z}) \quad \text{on } [\bar{z}_i, \bar{z}_{i+1}], \\ \Delta H_{i-\frac{1}{2}} &= H_{i+\frac{1}{2}} - H_{i-\frac{1}{2}}. \end{aligned}\right\} \quad (34)$$

The new breakpoint sequence is defined then with the piecewise-linear function κ, where

$$\kappa(\bar{z}) = \int_0^{\bar{z}} [h(s)]^{1/k}\, \mathrm{d}s; \quad \kappa(1) = \int_0^1 [h(s)]^{1/k}\, \mathrm{d}s. \quad (35)$$

The iteration for $n = 1, 2, 3, \ldots$ is described by

$$\bar{z}_i^{(n)} = \frac{1}{\kappa(\bar{z})} \left[(i-1) \frac{\kappa(1)}{l^{(n)}} \right], \quad 1 \leqslant i \leqslant l^{(n)}+1, \quad (36)$$

where $l^{(n)}$ is the new number of subintervals.

Number of iterations	$-\frac{1}{2}H(z_\infty)$	$\lvert\epsilon\rvert$	R_1	R_2
Uniform mesh	0.442185	—	0.80121×10^{-3}	0.45740×10^{-2}
1	0.442230	—	0.39920×10^{-3}	0.23161×10^{-3}
2	0.442227	0.275009×10^{-13}	0.50794×10^{-3}	0.29753×10^{-3}
3	0.442230	0.185264×10^{-13}	0.50158×10^{-3}	0.29704×10^{-3}
4	0.442232	0.186838×10^{-13}	0.49136×10^{-4}	0.29105×10^{-3}
Shooting (present)	0.442235	—	—	—
Zandbergen & Dijkstra	0.442237	—	—	—
Lentini & Keller	0.442237	—	—	—

TABLE 1. Effect of breakpoint grading on solution; branch I, $z_\infty = 15$, $N = 63$

Number of iterations	$-\frac{1}{2}H(z_\infty)$		
	$z_\infty = 15$	$z_\infty = 20$	$z_\infty = 25$
Uniform mesh	0.442185	0.44218	—
1	0.442230	0.442235	0.442237
2	0.442227	0.442234	0.442231
3	0.442230	0.442235	0.442236
4	0.442232	0.442234	0.442234
Shooting (present)	0.442235	0.442237	0.442237

TABLE 2. Effect of value of z_∞ on solution; branch I, $N = 63$

Number of iterations	$-\frac{1}{2}H(z_\infty)$			
	$N = 43$	$N = 63$	$N = 73$	$N = 95$
Uniform mesh	0.442101	0.442185	0.442202	—
1	0.442222	0.442230	0.442232	0.442236
2	0.442226	0.442227	0.442229	0.442235
3	0.442226	0.442230	0.442231	0.442235
4	0.442226	0.442232	0.442231	0.442228

TABLE 3. Effect of the value of N on solution; branch I, $z_\infty = 15$

Quite simply, the idea behind (32)–(36) is to place the breakpoints densely in subintervals where rapid change of the solution is anticipated. How far the iteration should proceed can be judged, for example, by observing the L_2 norm of the residue of the nonlinear system.

4. Results and discussion

The first task we set ourselves is demonstration of the accuracy of solution. We shall concentrate on the effect of three parameters: (i) the positioning of the far boundary z_∞; (ii) the number N of splines in the expansions; and (iii) the breakpoint

	$-\frac{1}{2}H(z_\infty)$	
s	Present solution	Zandbergen & Dijkstra
0	0.223861	0.2238617
0.005	0.220801	—
0.010	0.215594	—
0.015	0.208026	—
0.020	0.197853	0.197845
0.025	0.184783	—
0.030	0.168468	—
0.035	0.148479	—
0.040	0.124288	0.124313
0.045	0.905231	—
0.050	0.060464	—
0.055	0.018718	—
0.060	−0.030141	−0.030059

TABLE 4. Branch II of the basic flow; $N = 63$, $z_\infty = 60$

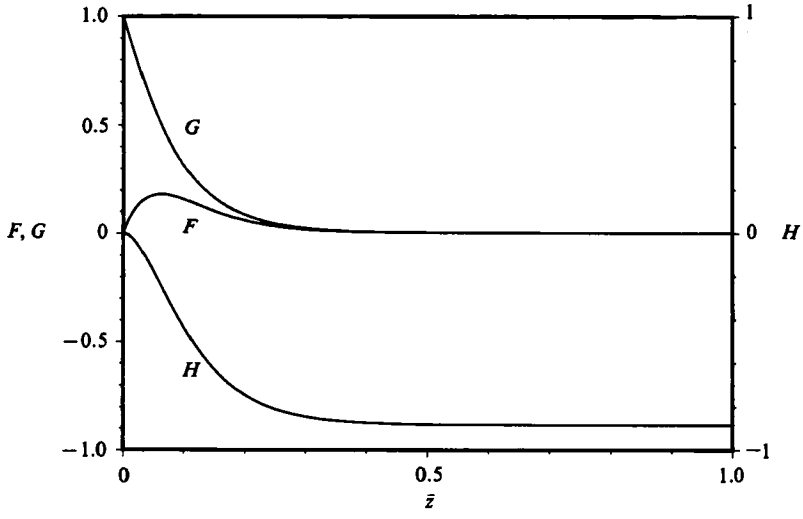

FIGURE 1. Branch I of the von Kármán swirling flow; $s = 0$.

sequence. The discussion on the influence these parameters have will be presented in reverse order.

The initial solution to the boundary-value problem (16) and (17) is obtained with uniform breakpoints. We then employ (33)–(36) to generate non-uniform breakpoint sequences. The goodness of solution is monitored by observing the value of the residues R_1 and R_2 and ϵ, the L_2 norm of the residue of the nonlinear system. The residues R_1 and R_2 have the following definitions (Zandbergen & Dijkstra 1977):

$$\left.\begin{aligned} R_1 &= \left| H''^2(0) - G'^2(0) - 4\int_0^\infty H(H''^2 - G'^2)\,\mathrm{d}z \right|, \\ R_2 &= \left| H''(0)\,G'(0) + \tfrac{2}{3}s^3 - s^2 + \tfrac{1}{3} - 4\int_0^\infty HH''G'\,\mathrm{d}z \right|. \end{aligned}\right\} \tag{37}$$

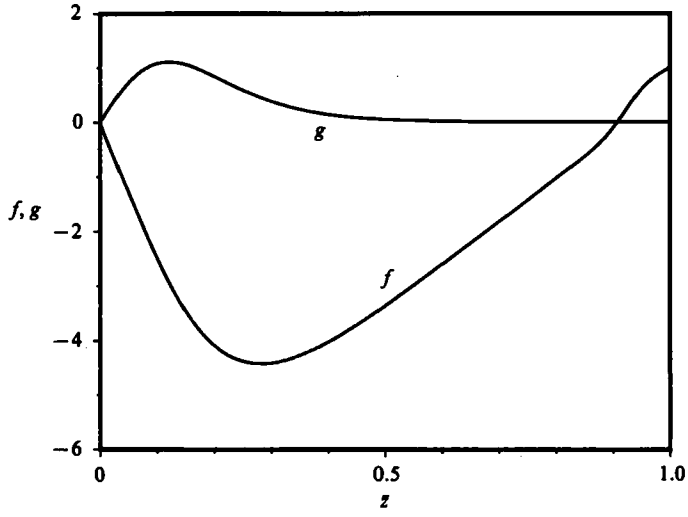

FIGURE 2. Branch I solution.

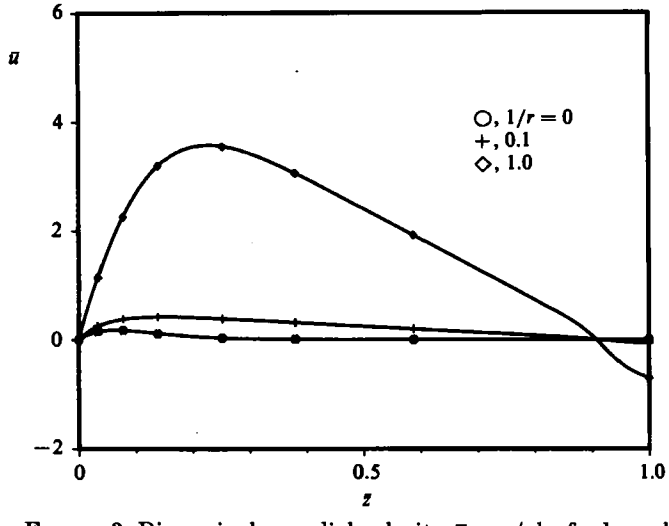

FIGURE 3. Dimensionless radial velocity $\bar{u} = u/x^{\frac{1}{2}}\omega$ for branch I solution, uniform streaming at infinity; $s = 0$, $\theta = \frac{1}{4}\pi$.

$\bar{z}$	$-\frac{1}{2}F$	G	$-\frac{1}{2}H$	f	g
)	0	1.0	0	0	0
).101922	-0.769229×10^{-1}	0.305583	0.222301	−2.51610	1.08797
).202665	-0.281637×10^{-1}	0.815955×10^{-1}	0.374909	−4.10850	0.832474
).304542	-0.790926×10^{-2}	0.211459×10^{-1}	0.424098	−4.40952	0.374448
).397707	-0.234408×10^{-2}	0.614416×10^{-2}	0.436914	−4.03762	0.147866
).502612	-0.586259×10^{-3}	0.152769×10^{-2}	0.440909	−3.33871	0.446386×10^{-1}
).623265	-0.118341×10^{-3}	0.308258×10^{-3}	0.441967	−2.42128	0.118231×10^{-1}
).707914	-0.383864×10^{-4}	0.100309×10^{-3}	0.442148	−1.75722	0.462389×10^{-2}
).825013	-0.801285×10^{-5}	0.212570×10^{-4}	0.442216	−0.830305	0.132947×10^{-2}
).905184	-0.26683×10^{-5}	0.736554×10^{-5}	0.442228	-0.410383×10^{-1}	0.602567×10^{-3}
1.0	-0.659625×10^{-6}	0.210909×10^{-5}	0.442232	1.0	0

TABLE 5. Flow induced by rotating disk in uniformly streaming fluid; branch I

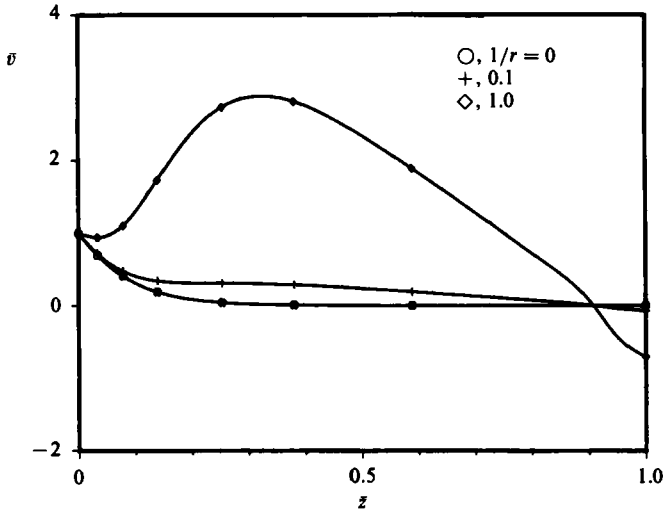

FIGURE 4. Dimensionless azimuthal velocity $\bar{v} = v/x^1\omega$ for branch I solution, uniform streaming at infinity; $s = 0$, $\theta = \frac{1}{4}\pi$.

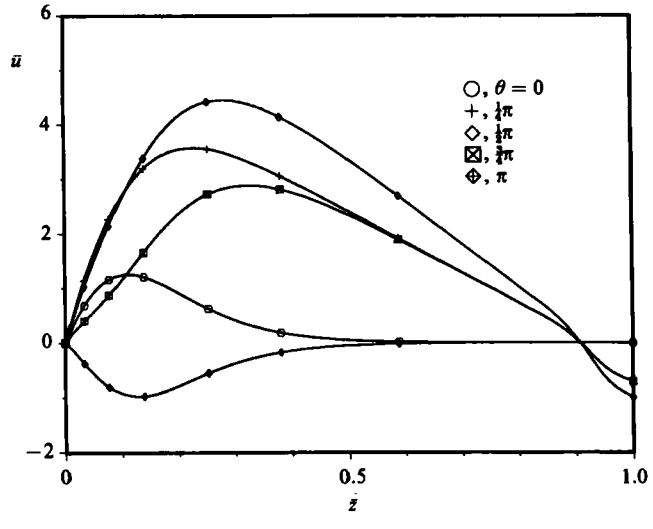

FIGURE 5. Dimensionless radial velocity $\bar{u} = u/x^1\omega$ for branch I solution, uniform streaming at infinity, $s = 0$, $r = 1$.

They are obtained from (16a, b) by simple algebraic manipulations, followed by integration.

Table 1 shows the effect of successive mesh grading on the values of the dimensionless axial flow at infinity, $H_\infty = H(z_\infty)$.

The results of Zandbergen & Dijkstra (1977), quoted in this table, were achieved in shooting via finite-difference discretization followed by Richardson extrapolation. The result of Lentini & Keller (1980a, b) was through finite-difference solution of the boundary-value problem.

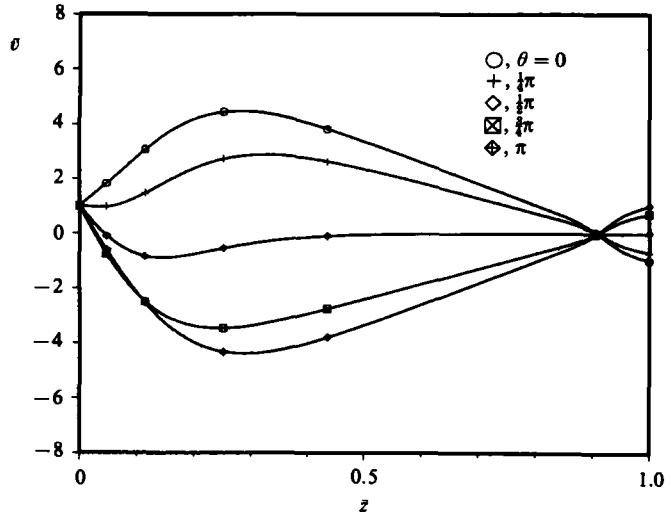

FIGURE 6. Dimensionless azimuthal velocity $\bar{v} = v/x^1\omega$ for branch I solution, uniform streaming at infinity; $s = 0$, $r = 1$.

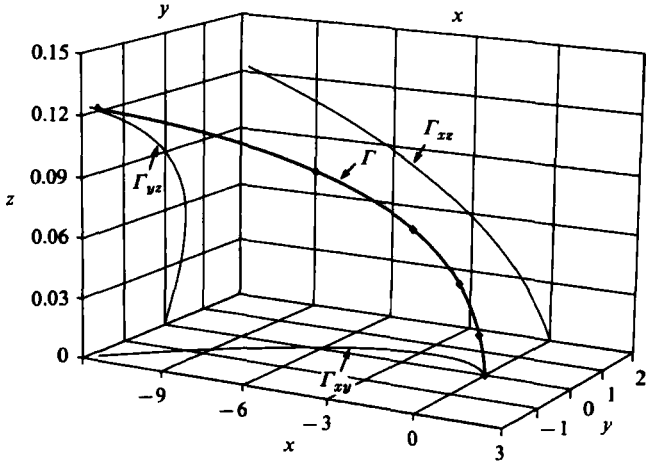

FIGURE 7. Branch I locus of stagnation points, uniform streaming at infinity; $u = v = 0$, $s = 0$.

In the calculations leading to table 1 we set the far boundary conditions at $z_\infty = 15$ and employ $N = 63$ splines in the expansion. Keeping N at this value and varying z_∞, we obtain the data of table 2. We monitored the values of the residues R_1 and R_2 and the residue ϵ; these showed convergence during iterations.

In our final illustration of accuracy of branch I, we keep the far boundary at $z_\infty = 15$ and vary the number N of splines in the expansions (21). The results of the calculation are shown in table 3. It seems that for single-precision calculation on a 32 bit machine best results are achieved with $63 < N < 73$, and for $N > 73$ there is a decrease of accuracy with increasing N. To fully utilize expansion in 95 splines we would have to revert to double precision on the PDP-10. Assuming that interpolation with B-splines produces errors proportional to $1/(N-1)^4$ (Hall 1968), the first row of table 3 yields $H(z_\infty) = 0.442222$ on the limit for uniform breakpoint distribution. The

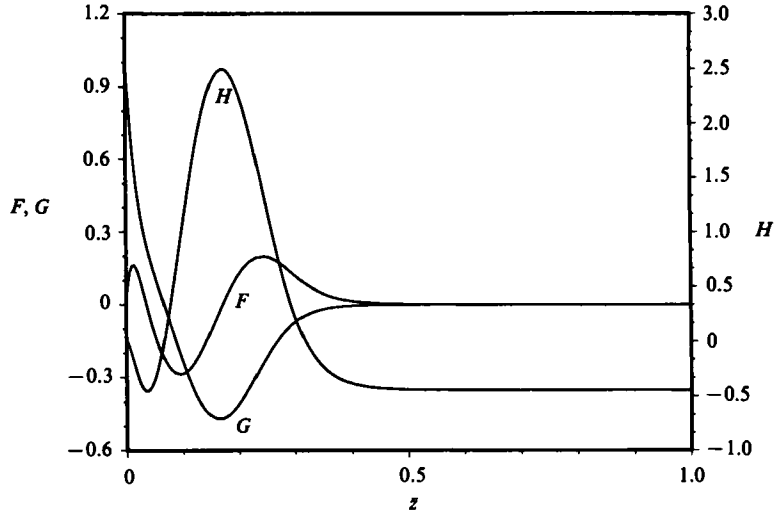

FIGURE 8. Branch II of the von Kármán swirling flow; $s = 0$.

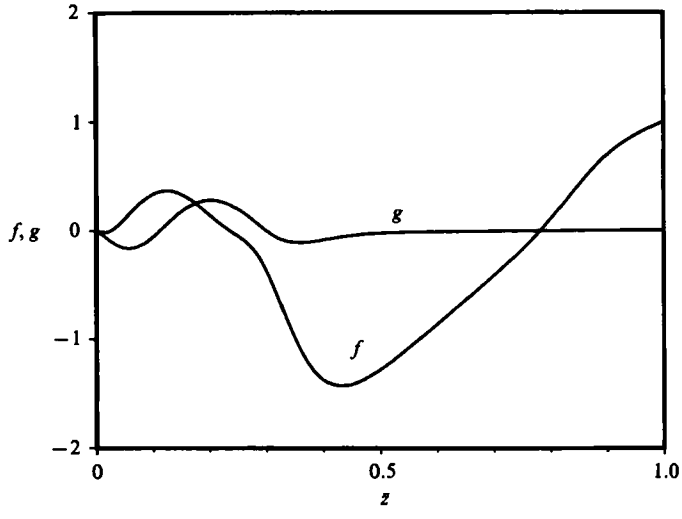

FIGURE 9. Branch II solution, uniform streaming at infinity; $s = 0$.

z	$-\frac{1}{2}F$	G	$-\frac{1}{2}H$	f	g
0	0	1.0	0	0	0
0.105789	0.139283	-0.269431	-0.623640	0.351949	-0.303695×10^{-1}
0.203469	-0.067563	-0.398178	-1.11058	0.130417	0.281305
0.304006	-0.056246	-0.665126×10^{-1}	-0.086306	-0.405928	-0.146166×10^{-1}
0.401941	-0.059352×10^{-1}	-0.500496×10^{-2}	0.196613	-1.37958	-0.831361×10^{-1}
0.453594	-0.153695×10^{-2}	-0.125002×10^{-2}	0.216976	-1.40772	-0.424869×10^{-1}
0.529329	-0.202789×10^{-3}	-0.163466×10^{-3}	0.22297	-1.16843	-0.175715×10^{-1}
0.613466	-0.209221×10^{-4}	-0.170823×10^{-4}	0.223779	-0.805925	-0.105211×10^{-1}
0.681057	-0.324374×10^{-5}	-0.277608×10^{-5}	0.223858	-0.500938	-0.791966×10^{-2}
0.791536	-0.088911×10^{-6}	-0.838308×10^{-7}	0.223873	-0.508031×10^{-1}	-0.536728×10^{-2}
1.0	-0.062088×10^{-7}	0.633599×10^{-7}	0.223874	1.0	0

TABLE 6. Flow induced by rotating disk in uniformly streaming fluid; branch II

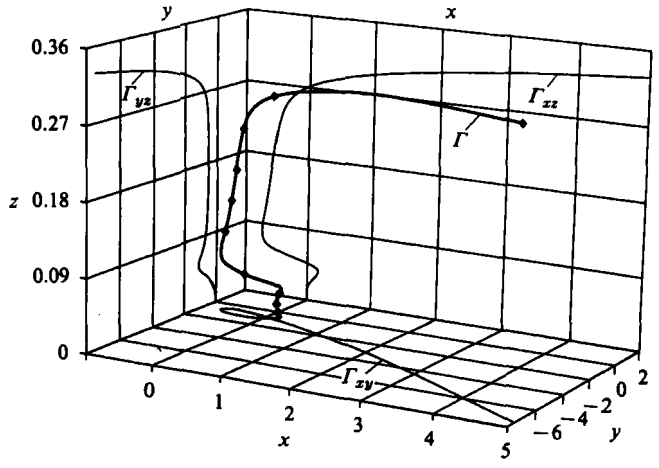

FIGURE 10. Branch II locus of stagnation points, uniform streaming at infinity; $u = v = 0$, $s = 0$.

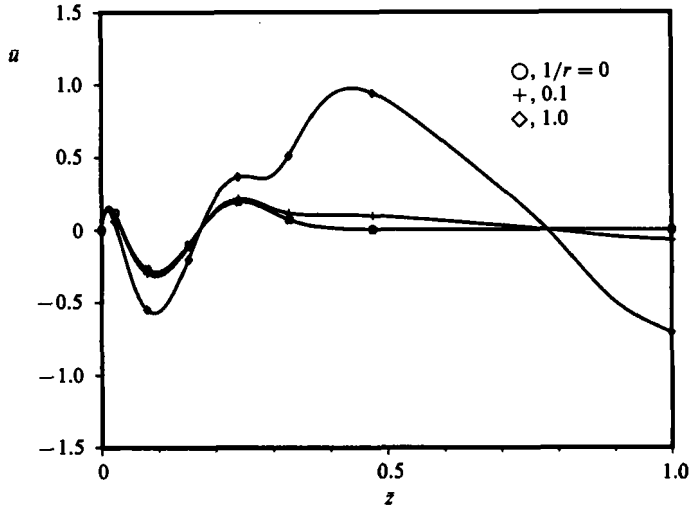

FIGURE 11. Dimensionless radial velocity $\bar{u} = u/x^1\omega$ for branch II solution, uniform streaming at infinity; $s = 0$, $\theta = \frac{1}{4}\pi$.

same data in Richardson extrapolation (Kopal 1961) leads to $H(z_\infty) = 0.442249$ from two points and to $H(z_\infty) = 0.442247$ from three points.

Table 4 compares our results for branch II with that of Zandbergen & Dijkstra (1977) at various values of s. In order to save computer time, the breakpoint distribution was optimized only at $s = 0$ and then kept invariant during continuation in s from $s = 0$ to 0.055. By continuation we refer to the process whereby the solution at some s provides the starting conditions for Newton's iteration at $s + \Delta s$. To reach $s = 0.06$ from $s = 0$ we took 12 steps, as shown in table 4. Our goal here was to reach $s = 0.06$; thus at this value of the ratio of rotational speed we again optimized the distribution of breakpoints. The value quoted at $s = 0.06$ in table 4 was obtained on an optimally graded mesh.

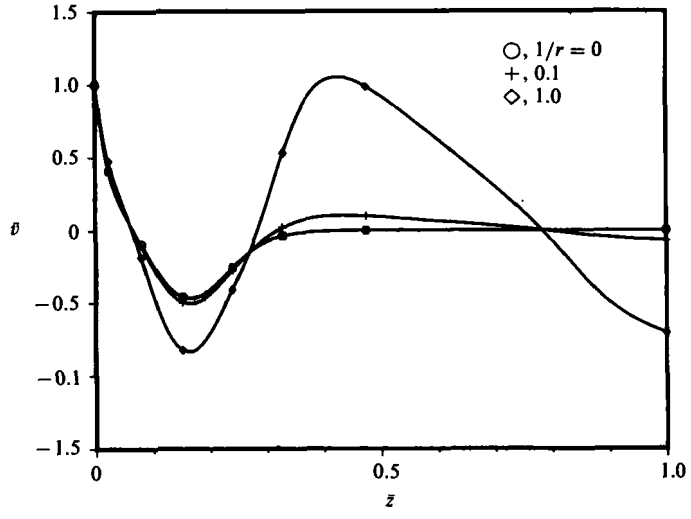

FIGURE 12. Dimensionless azimuthal velocity $\bar{v} = v/x^1\omega$ for branch II solution, uniform streaming at infinity; $s = 0$, $\theta = \frac{1}{4}\pi$.

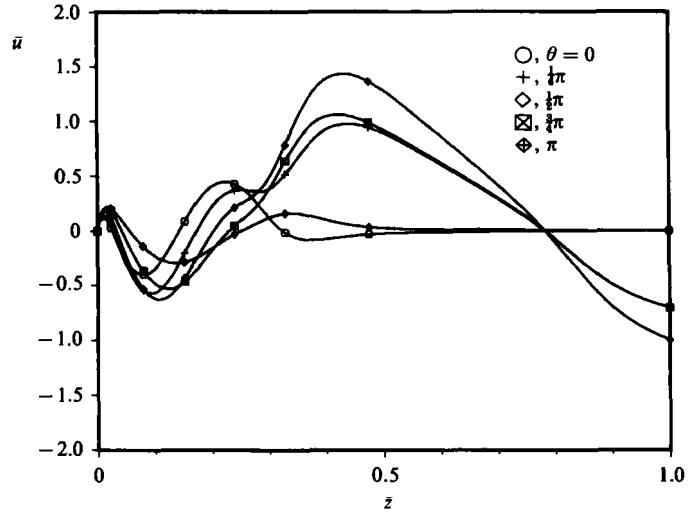

FIGURE 13. Dimensionless radial velocity $u = u/x^1\omega$ for branch II solution, uniform streaming at infinity; $s = 0$, $r = 1$.

In the first instance we investigate the flow that is induced by a rotating disk when it is placed in a fluid streaming uniformly in the $y < 0$ direction and having a velocity $\{0, -(\nu\omega)^{\frac{1}{2}}C, 0\}$. The boundary conditions satisfied by this flow are: (*a*) no slip at the disk, (13*a*, *c*); and (*b*) uniform velocity at infinity, (13*b*) and (14) together with $s = 0$. Figures 1 and 2 display the functions $\{F, G, H\}$ and $\{f, g\}$ respectively, for branch I of the solution. The corresponding numerical values are listed in table 5. The non-dimensional radial velocity $\bar{u} = u/x^1\omega$ is shown in figure 3 at $\theta = \frac{1}{4}\pi$ for various values of the non-dimensional distance from the axis of disk rotation. Far from the axis, $r \to \infty$, the flow appears to be the classical von Kármán solution, but this

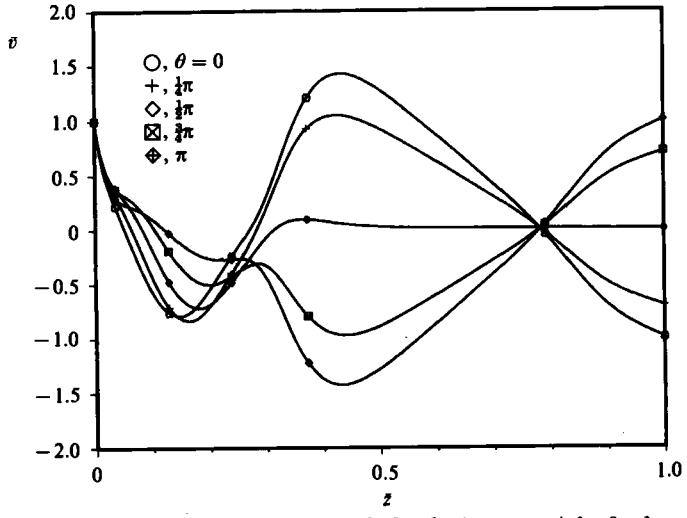

FIGURE 14. Dimensionless azimuthal velocity $\bar{v} = v/x^1\omega$ for branch II solution, uniform streaming at infinity; $s = 0$, $r = 1$.

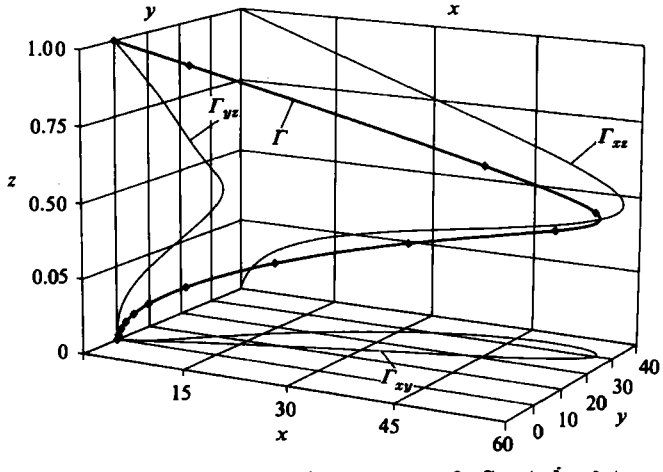

FIGURE 15. Branch I locus of stagnation points; $u = v = 0$, $C = 1$, $\hat{l} = 0.1$, $s = 0.02$.

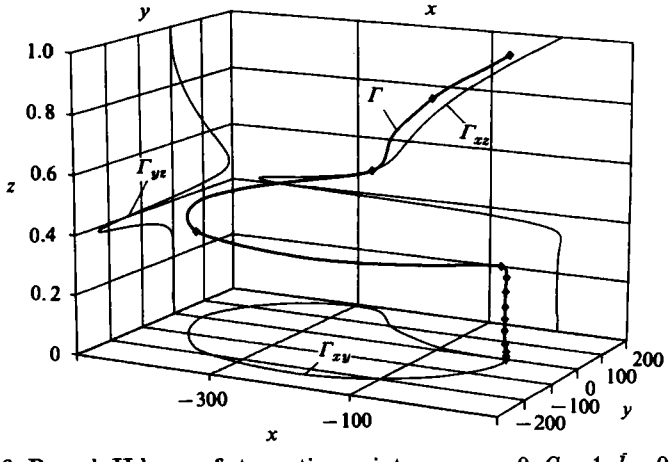

FIGURE 16. Branch II locus of stagnation points; $u = v = 0$, $C = 1$, $\hat{l} = 0.1$, $s = 0.02$.

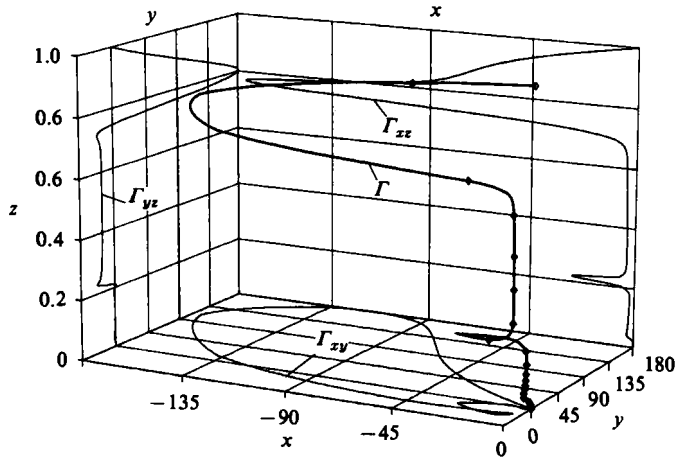

FIGURE 17. Branch III locus of stagnation points; $u = v = 0$, $C = 1$, $\bar{l} = 0.1$, $s = 0.02$.

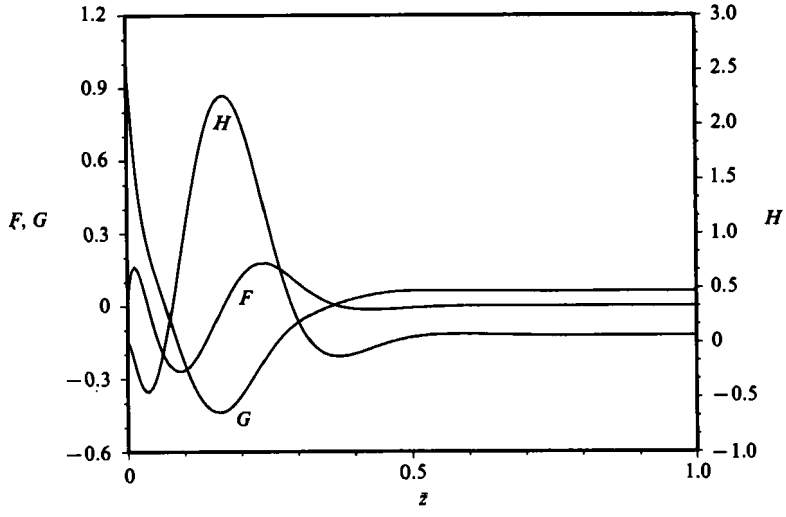

FIGURE 18. Branch II of the von Kármán swirling flow; $s = 0.06$.

appearance is misleading and is due to the fact that in the non-dimensional plot the contribution of $\{f(z), g(z)\}$ is lessened as there is division by r, (10), making it appear insignificant. As we approach the centre of rotation, however, even this superficial similarity of our flow to the von Kármán solution vanishes. We may remark here that the gradient of the non-dimensional velocity goes to zero as $z \to \infty$, and there is no shear layer at infinity. That this is not shown well in figure 3 is simply due to plotting $0 \leqslant z \leqslant \infty$ onto the unit interval. Remarks identical to these may also be made for figure 4, which shows the non-dimensional azimuthal velocity $\bar{v} = v/x^1\omega$. Figures 5 and 6 contain again the non-dimensional velocity components $\bar{u}$ and $\bar{v}$ respectively, but this time the distance from the centre of rotation is fixed at $r = 1.0$ and the profiles are shown as the observer sees them while moving along the unit circle from $\theta = 0$ to $\theta = \pi$. The velocity component $\bar{u}$ satisfies the von Kármán condition as $z \to \infty$ only at $\theta = 0$, while the far boundary condition of the classical solution is satisfied by $\bar{v}$ only at $\theta = \pm\frac{1}{2}\pi$. In all other positions the solutions exhibit less of a

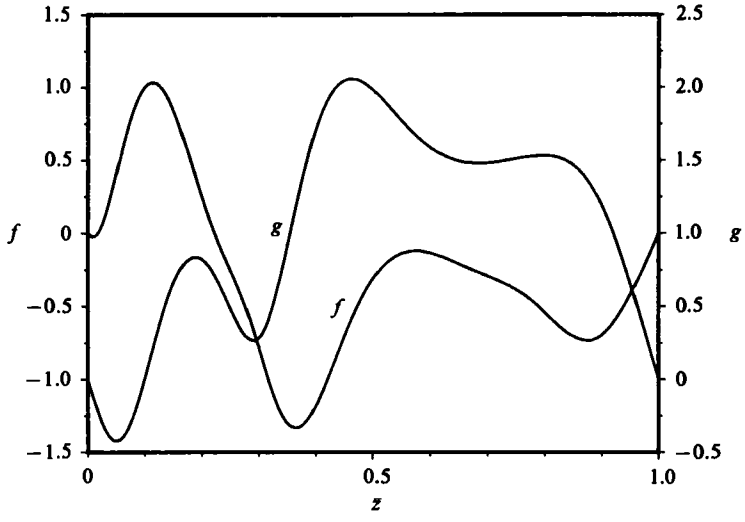

FIGURE 19. Branch II solution; $C = 1$, $\bar{l} = 0.1$, $s = 0.06$.

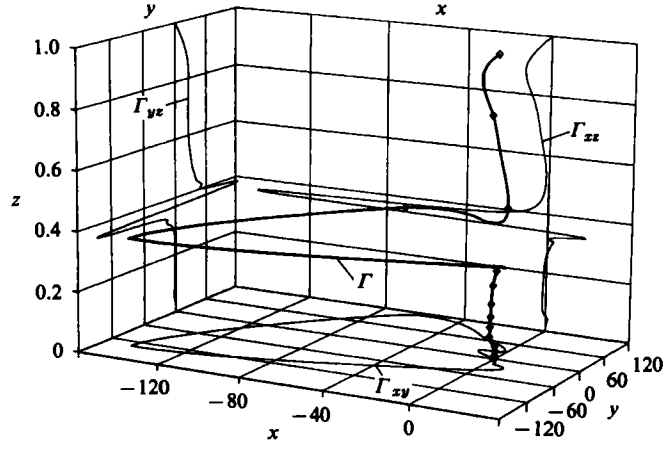

FIGURE 20. Branch II locus of stagnation points; $u = v = 0$, $C = 1$, $\bar{l} = 0.01$, $s = 0.06$.

boundary-layer structure than do the classical profiles. At $r = 1.0$ and $\theta = \frac{1}{2}\pi$ the rotation of the fluid is in opposition to disk rotation, except in a narrow layer adjacent to the disk.

Figures 5 and 6 show the velocity-profile development experienced by the observer moving along the circle $r = 1.0$ in the positive direction from $\theta = 0$. Since now $V \to 0$ as $z \to \infty$, the distance between the centre of rotation and the stagnation point increases out of bound as $z \to \infty$. This is indicated in figure 7, an isometric plot of the locus of stagnation points Γ. The coordinates of the stagnation points, which are defined here through $u = v = 0$, are given by:

$$\left.\begin{aligned} \theta^* &= \tan^{-1}\frac{F(z)f(z)+G(z)g(z)}{G(z)f(z)-F(z)g(z)}, \\ r^* &= \frac{f(z)\sin\theta^* - g(z)\cos\theta^*}{F(z)}. \end{aligned}\right\} \tag{38}$$

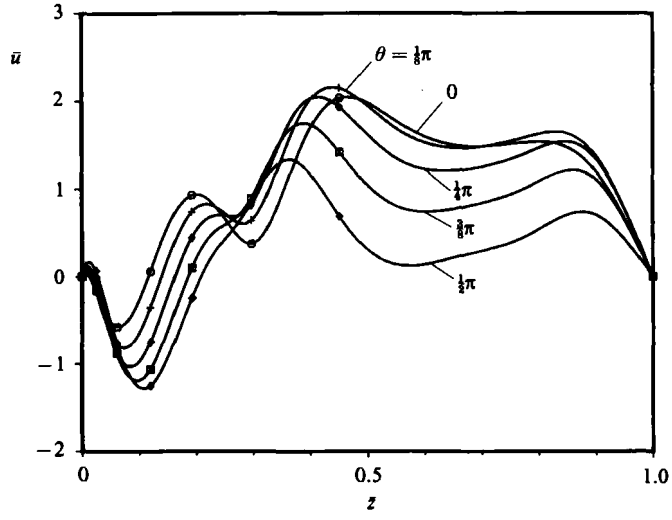

FIGURE 21. Dimensionless radial velocity $\bar{u} = u/x^1\omega$ for branch II; $C = 1$, $l = 0.1$, $s = 0.06$, $r = 1$.

Figure 7 also contains the projection of the locus of stagnation points Γ onto the coordinate planes of the Cartesian system $\{x, y, z\}$. The locus has one point in the $\{0, 0, 0\}$-position, and as $z \to \infty$ the distance between Γ and the rotational axis grows out of bound monotonically.

Branch II of the functions $\{F, G, H\}$ is shown in figure 8. The main feature of the second branch in comparison with branch I is the creation of two cells. A cell is identified as a region that is bounded by $z =$ constant planes on which the axial velocity vanishes. In the innermost cell adjacent to the disk the axial velocity is negative, i.e. towards the disk. The fluid is thrown outwards near the disk, and return flow is made in the upper half of the cell. The fluid rotates in the same direction as the disk, but its velocity decreases with z, to vanish at the cell boundary where $w = 0$. In the second cell, encountered as one moves further away from the disk, the axial velocity is positive and the circulation in the cell is clockwise when viewed along the θ-axis in the positive direction. The rotation of the fluid here opposes that of the disk. In the outermost region the fluid moves towards the disk with a velocity that approaches -0.223861 from above as $z \to \infty$, and is being thrown outward in the radial direction, its rotational velocity opposing that of the disk once more. The functions $f(z)$ and $g(z)$ are displayed in figure 9; the boundary condition at $z \to \infty$ is uniform streaming with velocity $\{0, -(\nu\omega)^{\frac{1}{2}}C, 0\}$. Table 6 lists the numerical values of the complete solution at selected breakpoints. The locus of stagnation points $u = v = 0$ for branch II is shown in figure 10. The projection onto the disk, i.e. the (x, y)-plane, is no longer a simple curve: it exhibits a single loop.

Figure 11 and 12 show the velocity components $\bar{u}$ and $\bar{v}$ respectively, at various radial positions along the ray $\theta = \frac{1}{4}\pi$. Figures 13 and 14 show velocity development as the observer moves along the $r = 1$ circle in the positive θ-direction. It may be seen that superposition of the velocity $\{(\nu\omega)^{\frac{1}{2}}g(z), -(\nu\omega)^{\frac{1}{2}}f(z)\}$ does not alter the basic cell structure of the flow, but it does change the magnitude and even the direction of the swirling motion within the cells.

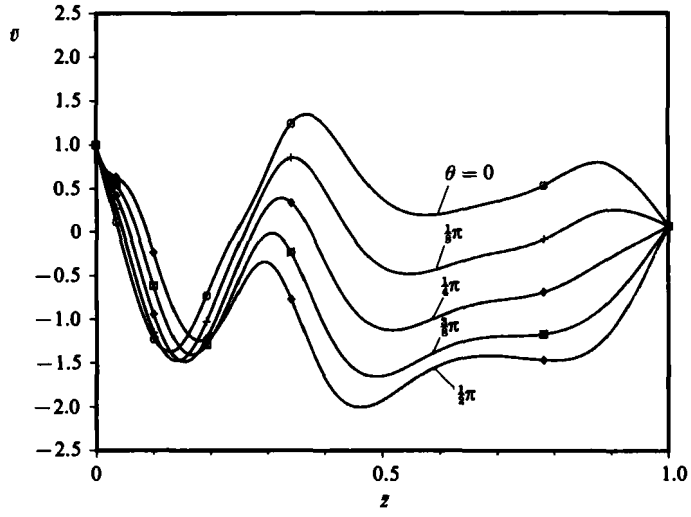

FIGURE 22. Dimensionless azimuthal velocity $\bar{v} = v/x^1\omega$ for branch II; $C = 1$, $\bar{l} = 0.1$, $s = 0.06$, $r = 1$.

For $s \neq 0$ we have

$$\lim_{z\to\infty} \frac{|q|}{|V|} = 0,$$

and consequently the distance between the axis of rotation and the locus of stagnation points goes to zero as $z \to \infty$.

The remaining solutions were obtained under the conditions (15*a*, *b*). Figures 15–17 show isometric plots of the locus Γ for $s = 0.02$ and branches I, II and III. We observe that the projection of the locus onto the disk is a closed curve consisting of one or more loops, the number of loops depending on the branch number.

Figures 18–20 display various plots of the branch II solution at $s = 0.06$. Figure 18 contains $\{F, G, H\}$ of the von Kármán swirling flow. The Cartesian components of the superposed velocity are shown in figure 19. The corresponding stagnation point locus is shown in figure 20. These solutions were obtained by continuation in s from $s = 0$. Figures 21 and 22 show the velocity development with θ on the unit circle.

5. Conclusions

We have demonstrated in this paper the existence of a set of hitherto unknown solutions to the Navier–Stokes equations. These solutions depend on, and are continuous in, a parameter C. As $C \to 0$ the asymmetric solutions degenerate into the axisymmetric solutions of von Kármán. Thus the von Kármán solutions are never isolated in the sense that there are asymmetric solutions arbitrarily close by.

The new asymmetric solutions described in this paper are the results of superposition of the von Kármán swirling flows and a pseudoplane flow that exhibits uniform velocity in planes parallel to the disk. The Cartesian components of this velocity $\{(\nu\omega)^{\frac{1}{2}} g(z), -(\nu\omega)^{\frac{1}{2}} f(z)\}$ are defined by two coupled linear equations, the coefficients of which depend on the solution of the von Kármán swirling flow. A subset of the solutions obtained here corresponds to flow induced by the rotation of a disk when the latter is placed in a fluid that is moving with a constant uniform velocity.

REFERENCES

BERKER, R. 1979 A new solution of the Navier–Stokes equation for the motion of a fluid contained between two parallel planes rotating about the same axis. *Arch. Mech. Stosowanej* **31**, 265–280.

DE BOOR, C. 1978 *A Practical Guide to Splines*. Springer.

DIJKSTRA, D. 1980 On the relation between adjacent inviscid cell type solutions to the rotating-disk equations. *J. Engng Maths* **14**, 133–154.

HALL, C. A. 1968 On error bounds for spline interpolation. *J. Approx. Theory* **1**, 209–218.

HASTINGS, S. P. 1970 An existence theorem for some problems from boundary layer theory. *Arch. Rat. Mech. Anal.* **38**, 308–316.

KÁRMÁN, T. VON 1921 Über laminare and turbulente Reibung. *Z. angew. Math. Mech.* **1**, 233–252.

KOPAL, Z. 1961 *Numerical Analysis*. Chapman & Hall.

LAI, C.-Y., RAJAGOPAL, K. R. & SZERI, A. Z. 1984 Asymmetric flow between parallel rotating disks. *J. Fluid Mech.* **146**, 203–225.

LAN, C. C. 1971 On functional differential equations and some boundary layer problems. *Arch. Rat. Mech. Anal.* **42**, 24–39.

LENTINI, M. & KELLER, H. B. 1980*a* The von Kármán swirling flows. *SIAM J. Appl. Maths* **38**, 52–64.

LENTINI, M. & KELLER, H. B. 1980*b* Boundary value problems on semi-infinite intervals and their numerical solution. *SIAM J. Numer. Anal.* **17**, 577–603.

MCLEOD, J. B. 1971 The existence of axially symmetric flow above a rotating disk. *Proc. R. Soc. Lond.* A **324**, 391–414.

PARTER, S. V. & RAJAGOPAL, K. R. 1984 Swirling flow between rotating plates. *Arch. Rat. Mech. Anal.* **86**, 305–315.

ROGERS, M. H. & LANCE, G. N. 1960 The rotationally symmetric flow of a viscous fluid in the presence of an infinite rotating disk. *J. Fluid Mech.* **7**, 617–631.

RUSSELL, R. D. & CHRISTIANSEN, J. 1978 Adaptive mesh selection strategies for solving boundary value problems. *SIAM J. Numer. Anal.* **15**, 59–80.

WEIDMAN, P. D. & REDEKOPP, L. G. 1975 On the motion of a rotating fluid in the presence of an infinite rotating disk. In *Proc. 12th Biennial Fluid Dynamics Symp., Bialowieza, Poland.*

ZANDBERGEN, P. J. & DIJKSTRA, D. 1977 Non-unique solutions of the Navier–Stokes equations for the Kármán swirling flow. *J. Engng Maths* **11**, 167–188.